The South Georgia Wave Experiment (SG-WEX): Radiosonde observations of gravity waves in the lower stratosphere. Part 1: Energy density, momentum flux and wave propagation direction

Tracy Moffat-Griffin[1], Corwin J. Wright[2], Andrew C. Moss[2] John C. King[1], Steve R. Colwell[1], John K. Hughes[3], Nicholas J. Mitchell[2]

[1]Atmosphere, Ice and Climate Group, British Antarctic Survey, Cambridge, United Kingdom, CB3 0EJ

[2] Centre for Space, Atmospheric and Ocean Science, Department of Electronic and Electrical Engineering, University of Bath, Bath, United Kingdom, BA2 7AY

[3] School of Earth and Environment, University of Leeds, United Kingdom, LS2 9JT

Correspondence to: Tracy Moffat-Griffin (tmof@bas.ac.uk)

Keywords: gravity waves, lower stratosphere, radiosondes, ANGWIN

Running title: SG-WEX: radiosonde gravity wave observations part1

Abstract. Gravity waves play a critical role in the transport of energy and momentum throughout the atmosphere. It has been suggested that small mountainous islands located in regions of strong winds may generate significant fluxes of these waves. Such fluxes would be important because these islands are not well resolved in global circulation models. Thus, there is a need to determine the magnitude and variability of gravity wave generated from such islands: South Georgia (54°S, 37°W) has the highest mountains of these islands. Here, we present the first report of gravity waves measured by radiosondes over South Georgia. The measurements were made in two intensive campaigns as part of the South Georgia Wave

This article has been accepted for publication and undergone full peer review but has not been through the copyediting, typesetting, pagination and proofreading process, which may lead to differences between this version and the Version of Record. Please cite this article as doi: 10.1002/qj.3181

EXperiment (SG-WEX), a multi-instrument and modelling campaign investigating gravity waves above South Georgia. The two intensive radiosonde campaigns were held in 2015, one in January and one in June/July, totalling 89 successful launches. We use these new observations to determine gravity wave properties in the lower stratosphere. The summer campaign observed an average wave energy density (kinetic+potential+vertical) of 3.6 JKg^{-1} and an average pseudo-momentum flux of 2.3 mPa . In the winter campaign the values observed were larger; an average wave energy density of 8.4 JKg^{-1} and an average pseudo-momentum flux of 8.7 mPa . Strikingly, analysis reveals that in winter 66% of waves were propagating downwards, in summer only 8% did so. These results suggest that there may be additional sources of waves in the winter stratosphere. We propose that the differences between wave properties observed during the summer and winter campaigns are due to a complex combination of factors including differences in surface wind conditions (linked to orographic wave generation), frequency of storms and the proximity of the Polar stratospheric jet. These results demonstrate a large increase in gravity wave activity in winter above South Georgia.

1 Introduction

Gravity waves are launched by sources mostly found in the lower atmosphere (e.g. strong winds blowing over mountains, the polar stratospheric jet and storm systems). These waves naturally grow in amplitude as they ascend into the upper atmosphere (assuming no dissipation) transporting large amounts of energy and momentum as they do so. When they dissipate, like a wave breaking on the beach, they deposit their energy and momentum locally in the atmosphere, driving atmospheric circulation (Fritts and Alexander, 2003). These atmospheric waves are relatively small-scale (10 km-1000 km horizontal wavelength) and, as such, a significant part of their spectrum have to be represented in global circulation and

numerical weather prediction models through parameterisations. Despite the importance of gravity waves there is a lack of knowledge about the variability of their sources. There is a need for observations to help understand this variability and refine the model parameterisations (Alexander et al., 2010a).

One example of a deficiency arising due to incomplete gravity wave representation in models is the "missing" gravity wave momentum flux in models around latitude 60°S. This momentum flux deficit is thought to be responsible for the delayed spring break-up of the polar vortex and the for polar middle atmosphere being too cold in most models (McLandress et al., 2012). Recent satellite studies have shown that small, mountainous islands, in regions of strong winds, are likely to be an intense source of gravity wave activity (Alexander et al., 2009a;Alexander and Grimsdell, 2013;Hoffmann et al., 2016). It is thought that they contribute significantly to the "missing" momentum flux in atmospheric models over the Southern Ocean, an estimate of the magnitude of this missing flux is a zonally averaged value of ~10mPa (McLandress et al., 2012). One of the small mountainous islands in the Southern Ocean that has been studied with satellite observations is South Georgia (Fig. 1, taken from (Bannister, 2015)). This is a very mountainous island and is subject to the strong Antarctic circumpolar winds. Its orientation is such that, on occasion, these winds can cross the mountain range perpendicular, ideal conditions for generating orographic gravity waves. Studies of the gravity wave activity above South Georgia have shown that it can be a source of intense gravity waves. However, satellites alone cannot view the whole gravity wave spectrum e.g. even combined satellite observations can't capture the short vertical wavelength gravity waves (less than 5 km) across a wide range of horizontal wavelengths (5 km – 200 km) (Wright et al., 2016). In order to study the gravity wave field of such an island in detail, and to determine the gravity wave momentum flux it generates, a combined instrument-modelling approach is needed.

The South Georgia Wave EXperiment (SG-WEX) aims to investigate the nature, variability and influence on atmospheric circulation of the gravity wave field above South Georgia using a range of modelling, satellite and ground based observations. Radiosondes provide a complimentary dataset to the satellite observations as they can observe the part of the gravity wave spectrum that satellites cannot capture, i.e. short vertical wavelength waves. Part of SG-WEX involved two radiosonde campaigns being undertaken, one in austral winter, one in austral summer (note: all references to summer and winter in this paper from now on refer to the austral summer and austral winter respectively). This paper (part one of two) presents the radiosonde gravity wave observations from King Edward Point (KEP) research station on South Georgia, focussing on the energy density, momentum flux and vertical and horizontal direction of propagation of waves in the lower stratosphere. Part two will focus on the individual properties of the waves detected, e.g. phase speeds, wavelengths.

2 Observing gravity waves above South Georgia with radiosondes

2.1 South Georgia climatology and terrain

South Georgia is situated 1200 km southeast of the Falkland Islands at 54º S, 37º W. The main island of South Georgia is approximately 170 km long and between 2 and 40 km wide. The island is very mountainous with the highest mountain on the island a height of 2.9 km, (GSGSSI, 2016). KEP station is located on the northern shore of South Georgia in a bay surrounded by high mountains (Fig.2).

The local climate of South Georgia is classified as sub-Antarctic i.e. a wet, cold windy environment which also has substantial glaciation. This climate is due to its location in the Southern Ocean; it is located in a region of strong eastward winds and, with its knife-like terrain, it acts a barrier to these winds, experiencing frequent storm systems. These winds mean that the western side of the island often experience more severe weather conditions than

the eastern side, as it is exposed to the fast, eastward moving depressions that track though this region of the Southern Ocean.

2.2 South Georgia radiosonde campaigns

South Georgia, due to its nature as a small, remote, mountainous island, is difficult to access. A semi-regular monthly ship route runs between KEP and the Falkland Islands throughout the year, a journey which can take over 4 days. The site of KEP itself presents its own difficulties as a radiosonde launch site: depending on wind direction the radiosonde could be taken behind the mountains, thus losing signal and data. The island also experiences strong surface winds that can hamper the launch of the radiosonde balloon. However, during January, June and July 2015 two successful radiosonde campaigns were undertaken from KEP, with twice daily launches at 11UT and 23UT as standard. Additional radiosondes were launched to coincide with overpasses by the A-Train satellite constellation or when forecasts predicted strong winds perpendicular to the spine of the island (conditions suitable for strong orographic wave generation). Each radiosonde also included a parachute so descent data were also recorded. For this paper only results from the ascent data are used as the descent rate data is at a much lower height resolution and not suitable for the analysis technique used here.

The radiosondes used were the Vaisala RS92-SGP model (Vaisala, 2013). The radiosonde data are composed of altitude profiles of temperature, wind speed, wind direction, pressure, humidity and dew point at both 10 second and 2 second resolution. The 2 second resolution data also contains the balloon ascent rate. For both campaigns a mix of 500g and 800g balloons were available, with 500g balloons having an expected 26 km burst altitude and 800g balloons having an expected 28 km burst altitude (although no difference in burst altitude is detectable in the campaign data). 800g balloons were used when the wind direction forecasts predicted favourable conditions for strong mountain wave generation.. Of the 89

successful launches 70 launches reached above the tropopause (~10 km altitude) and 56 reached 25 km or above.

Figures 3a and 3b shows all the temperature profiles from the summer and winter campaigns respectively. The tropopause can be clearly shown to be around 10 km altitude. From the radiosonde wind direction and wind speed data we can also derive the balloon trajectory. Figure 4 shows the balloon trajectories from KEP for the two campaigns. In winter the balloons travel further horizontally from KEP (up to 650 km compared with ~200 km maximum during the summer campaign), due to the stronger eastward winds present at this time of year in the stratosphere.

3 Methods

3.1 Gravity wave energy density

Gravity wave energy density is a measure of gravity wave activity (Allen and Vincent, 1995). It can be calculated using radiosonde profiles of temperature and wind perturbations due to gravity waves. Here, the perturbations of temperature and wind are determined by fitting a third-order polynomial to the profile and then subtracting this from the original profile, thus removing the background atmosphere and leaving only gravity waves in the profile. This fitting method is applied only to the height range of the profile that is of interest: for this paper between 12 km and 25 km altitude, allowing us to detect gravity waves with a vertical wavelength less than 13 km. An example fit and residual perturbation profile for temperature and wind can be seen in Fig. 5.

The total energy density, E_T can be calculated using Eq. (1). The three terms on the left hand side are as follows: horizontal kinetic energy density (KE), potential energy density (PE) and

vertical kinetic energy density (VE), where u', v', w' and $\hat{T}'$ are the zonal, meridional and vertical wind and the normalized temperature perturbation (temperature perturbation normalized by the background temperature) profiles respectively and N is the Brunt-Väisälä frequency. An overbar signifies averaging over height.

$$E_T = \frac{1}{2}\left(\overline{u'^2} + \overline{v'^2}\right) + \frac{1}{2}\frac{g^2}{N^2}\overline{\hat{T}'^2} + \frac{1}{2}\overline{w'^2} \quad (1)$$

Using the radiosonde ascent rate the vertical wind velocity perturbation can be calculated. For the SG-WEX data the vertical wind velocity perturbation (w') can be determined by taking the 2 second resolution ascent rate and removing the frequencies associated with the balloon's motion through the atmosphere (Gong and Geller, 2010). The perturbation in the resulting time series can then be assumed to be a reasonable representation of the perturbation of vertical wind due to gravity waves (Zhang et al., 2012). Although the vertical energy term is quite small in magnitude compared to the kinetic and potential energy values it is very sensitive to the high frequency part of the gravity wave spectrum (Geller and Gong, 2010) and can provide important information about the frequency composition of the wave field.

3.2 Gravity wave momentum fluxes

Gravity waves have an associated vertical flux of horizontal momentum (hereafter referred to as momentum flux). It is this momentum that is transferred to the atmospheric flow when the waves break, driving the atmospheric circulation (Fritts and Alexander, 2003).

The perturbations of wind velocity and temperature can be used, through the use of the polarisation equations, to calculate the pseudo-momentum flux for each profile. (Vincent et al., 1997). The zonal pseudo-momentum flux is calculated using Eq. (2) (the meridional

pseudo momentum flux is calculated by replacing *u'* with *v'* in Eq. 2.) where $\hat{T}'_{+90}$ is the Hilbert transformed normalised temperature perturbation. The average spectral frequency ($\bar{\omega}$) is given by Eq. 3.

$$F_u = \overline{u'w'} = -\frac{\bar{\omega}g}{N^2}\overline{u'\hat{T}'_{+90}} \quad (2)$$

$$\bar{\omega} = N\frac{(p-1)}{(2-p)}\hat{f}^{p-1}\left(1-\hat{f}^{p-2}\right) \quad (3)$$

Where $\hat{f} = \frac{f}{N}$ and p = 5/3 (Vincent et al., 1997).

3.3 Gravity wave propagation directions

The horizontal and vertical direction of propagation of a gravity wave observed in radiosonde data can be determined using a hodograph technique; where the meridional and zonal wind perturbations over the altitude range are plotted against each other, forming an elliptical or circular shape (Wang and Geller, 2003). The direction of rotation of the resulting hodograph gives vertical propagation information: if it is anti-clockwise then the wave has upward energy propagation, if it is clockwise then it has downward energy propagation. The horizontal direction of propagation of the wave is along the major axis of the hodograph ellipse. An example of a hodograph for a wave with downward energy propagation can be seen in Figure 6.

It is assumed, based on the results of previous studies (Moffat-Griffin et al., 2011;Zink and Vincent, 2001a), that the radiosonde will sample multiple gravity waves during its ascent.

Thus, if we wish to use the hodograph method to reliably determine each gravity wave's direction of propagation we need to first isolate the individual wave events.

A proven methodology to do this with radiosonde data is to use wavelet analysis, as detailed in Zink and Vincent, 2001. A Morlet wavelet transform is applied to the wind and temperature perturbations to identify the wave events in altitude and wavenumber space. An inverse wavelet transform (Torrence and Compo, 1998) is then applied to the region where the wave events exist, resulting in temperature and wind perturbation profiles associated with a single wave event. Where there are multiple wave events detected in one profile, (Moffat-Griffin et al., 2013) the Zink and Vincent method allows any overlapping waves (in either altitude or wavenumber space) to have their variance shared before reconstructing their perturbation profiles using the inverse wavelet transform, thus ensuring there is no contamination between the waves. The hodograph technique can then be applied to these data without risk of contamination of the results from other wave events.

4 Results

All results presented in this paper use ascent data from radiosondes that reached at least 25 km altitude. The lower boundary is taken to be 12 km so that it is above the potential distorting effects of the tropopause on the analysis techniques used. This constraint gives 24 radiosonde profiles in summer and 22 profiles in winter.

4.1 Energy density

The kinetic, potential and vertical energy density were calculated using each whole profile between 12 km and 25 km altitude. Geller and Gong (2010) have shown the kinetic energy is sensitive to low frequency gravity waves, potential energy to a mix of low and high frequency

waves and vertical energy to high frequency waves. By comparing all three values the frequency composition of the gravity wave field can be inferred.

Figures 7 and 8 show these three different energy density components for the summer and winter campaigns respectively. The most striking difference between the two datasets is the much higher values of all three energy measurements during the winter campaign compared to the summer campaign. Both seasons show day to day variability in gravity wave activity, with the variability being larger in the winter, i.e. standard deviation of kinetic energy density for the summer campaign is 0.5 JKg^{-1} but for the winter campaign is 2.2 JKg^{-1}.

During the summer all components of the gravity wave energy density are relatively constant in their magnitudes, implying a near constant gravity wave field of mixed frequencies. The exception to this is a period towards the end of the campaign, starting half way though the 17th January and extending until the 19th January. This small increase in KE, PE and VE occurs during one of the intensive campaigns where balloons were launched every 4 hours for 2 days.). The increase in energy densities isn't as large in KE as it is in PE and VE, suggesting a larger increase in higher frequency gravity waves (with intrinsic frequency (ω) tending towards the Brunt-Väisälä frequency (N)) than low frequency waves (with ω tending towards the inertial frequency (*f*)).

Figures 9a and 9b show time series of ERA-interim reanalysis data for the zonal and meridional wind components against altitude over KEP during the summer campaign (Figures 10a and 10b show the same but for the winter campaign). During the period of enhanced wave energy (17th-19th January) discussed above we see that the wind becomes more south-eastward, resulting in strong cross flow across the island. In addition during the same period there was a storm system that was moving close to and across South Georgia (the only one to come this close during the summer campaign), which resulted in increased surface and close

to surface wind speeds ((BAS), 2015). The storm system itself is a source of gravity waves but the increased wind speeds associated with it, combined with the wind direction, would have resulted in ideal conditions for strong orographic wave generation (Alexander et al., 2009a).

During the winter months the circumpolar winds are much stronger and more consistently eastward throughout the lower atmosphere than in the summer (compare Figures 9a and 10a). There are also more frequent, deeper, low pressure storm systems (Alexander and Grimsdell, 2013;Hoskins and Hodges, 2005;Jewtoukoff et al., 2015). Both of these factors, combined with favourable conditions for wave propagation to the stratosphere (i.e. eastward winds at all heights, compared with the summer where there is a critical level due to the wind reversal at ~22 km altitude), are likely to account for increased gravity wave activity seen in the winter.

During the winter campaign there is a lot of variability between the three energy densities, implying that different frequency gravity waves dominate on different days. The most distinct increase in energy density occurs between 28th June and 1st July for KE and PE with increased VE levels being seen 4 days before this date and until the end of the dataset. This period coincides with the wind being aligned in a favourable direction across the island (i.e. winds perpendicular to the mountainous spine of the island), the wind at the altitude above the mountains (~3 km) being strong and also storms passing directly over the island. These combination of factors would generate strong orographic waves and these are most likely the reason for the marked increase in energy density.

An additional characteristic of this period is that PE>KE for most of its duration. This contradicts linear gravity wave theory where we would expect to see the ratio of KE:PE to be between 2 and 1.67 (Nastrom et al., 1997). However, this ratio comes from a spectral approach and assumes that the waves are dominated by low frequency inertia waves, in the

case of orographic waves it might be expected that they have an intrinsic frequency quite high relative to *f,* so this ratio would not hold. The fact that PE stays greater than KE for a prolonged period also suggests that it is likely to be a real feature, and not down to contamination of the data (e.g. from the tropopause featuring in the temperature data, (Moffat-Griffin et al., 2011;Smith et al., 2008). Such features have been seen in other radiosonde studies (Sato and Yoshiki, 2008) and it has also been suggested from numerical studies that this scenario could arise when large amplitude gravity waves are present or gravity wave shearing is occurring (Fritts et al., 2006). As the zonal stratospheric winds during this time are so large (> 60 ms^{-1}) and there is a likelihood of strong orographic waves being generated at this time it could be that linear gravity wave theory no longer holds in this height region.

The differences seen between the summer and winter season at KEP are consistent with those from previous Antarctic and small Southern Ocean island radiosonde stratospheric gravity wave studies ((Murphy et al., 2014;Vincent et al., 1997;Yoshiki et al., 2004;Yoshiki and Sato, 2000;Zink and Vincent, 2001a;Moffat-Griffin et al., 2011;Moffat-Griffin et al., 2013;Innis et al., 2004)) where there is an increase in the wintertime values. However, each of these studies uses a slightly different method (e.g. use of whole profile compared with individual waves, use of lognormal statistics) and altitude range to calculate their energy density values. This can make comparison of the energy density magnitudes difficult. It has been shown that the use of lognormal statistics can reduce the estimate of energy density by around a factor of 2 (Murphy et al., 2014). There is also a reduction in energy density values when only using the individual waves in a profile compared to the whole profile (e.g Zink and Vincent (2001) compared to Vincent (1997)).

In Vincent (1997) the total energy density is calculated for summer and winter using the whole profile and over the same height range as this paper. The data used is from Macquarie

Island, a small island (less mountainous than South Georgia) at a latitude of 55°S. For summer they present a value of 4.2 JKg^{-1}, close to the value of 3.6 ± 0.5 JKg^{-1} for South Georgia. For winter a value of 6.7 JKg^{-1} is given, this is smaller than the South Georgia value of 8.4 ± 2.2 JKg^{-1} although within the standard deviation bounds of our result. Although the Macquarie Island results are seasonal averages and our values are two snapshots from part of each season the degree to which the South Georgia winter values of total energy density are larger does imply that South Georgia will have more gravity wave activity in winter months than Maquarie Island.

4.2 Gravity wave pseudo-momentum fluxes

Figures 11 and 12 show the meridional and zonal pseudo-momentum fluxes for the summer and winter campaigns respectively.

As expected from the analysis above, the pseudo-momentum flux values shown in Figures 11 and 12 are generally larger in winter than in summer: a summer campaign average of F_u = -2.19 mPa and F_v = -0.58 mPa compared to a winter campaign average of F_u = 6.36 mPa and F_v = -5.96 mPa. In the summer data we see the most variability in the pseudo-momentum flux at a time that corresponds directly with the increase seen in the energy density around the 18th January 2015. . The winter zonal pseudo-momentum flux is more consistently and stronger westwards than during the summer campaign, consistent with the deep persistent eastward winds that dominate in winter months. In both the meridional and zonal winter pseudo-momentum fluxes we see the largest values of flux occurring at the same time as the largest peak in energy density between the 28th June and 1st July.

The South Georgia results are compared to those values from Vincent (1997) (which use the same method of calculation and altitude range as this paper) in Table 1.

Both Islands have similar flux values for both seasons, although in winter it can be seen that the results from Vincent (1997) are larger in both the zonal and meridional directions. However, in the winter the South Georgia data has a large increase in energy density that has already been highlighted. It can be seen from Figure 12 that the associated pseudo-momentum flux with this event would dominate any averages. As the Macquarie data is from a seasonal value any such events may dominate their mean values too.

	Winter $F_{x\ (mPa)}$	Winter $F_{y\ (mPa)}$	Summer $F_{x\ (mPa)}$	Summer $F_{y\ (mPa)}$
South Georgia	-6.4	-5.9	-2.2	-0.5
Macquarie Island (results taken from Vincent (1997))	-9.3	-11	-2.6	-1.3

An analysis of AIRS satellite data in the region around South Georgia provided information on the winter monthly mean values of momentum flux (Alexander and Grimsdell, 2013). For June and July they found an average of 50 mPa, in this study we have an average magnitude momentum flux of 8.7 mPa. This is a much smaller value (although it is consistent with similar radiosonde studies) but several considerations have to be taken into account. Firstly the two instruments have very little overlap in terms of gravity waves they can observe (Wright et al., 2016) (satellites can see much longer vertical wavelength waves (12 km minimum compared with a maximum of 13 km for radiosondes). Secondly the satellite values are an average across a spatial region that will encompass much more wave activity than the radiosonde, on its single transit through the atmosphere, can observe. In this context the difference in magnitude between the two values is not unexpected. However, even though the

radiosonde winter monthly mean momentum flux is an order of magnitude smaller than the satellite observations, it does show that there is still a significant momentum flux being transported by the shorter vertical wavelength gravity waves.

4.3 Gravity wave direction of propagation

The previous sections used the whole radiosonde profile between 12 km and 25 km to estimate the energy densities and momentum flux of the gravity wave field in this region. In this section we use the individual wave packet profiles generated by the wavelet analysis to calculate the wave direction parameters.

Figures 13 and 14 show the horizontal directions of propagation for summer and winter respectively. The left-hand side of each figure shows the directions for downward propagating waves and the right shows directions for upward propagating waves. The horizontal direction of propagation is mainly westward in both seasons, but the distribution of upward and downward propagating waves is markedly different with the percentage of downward propagating waves increasing from 8% to 66% of the total observed waves from summer to winter.

The horizontal direction of propagation of the waves observed are consistent with what is expected due to the background wind conditions in the troposphere and stratosphere in the summer and winter. In winter there are stronger, more constant eastward winds (see Figure 10a), so the majority of eastward propagating waves are subject to critical level filtering (Whiteway and Duck, 1996) and do not reach the observation region. In the summer there is more variability in the direction of the wind (see Figure 9), so both eastward and westward propagating waves can make it though, although the majority are still westward propagating.

An interesting result is the difference in downward and upward propagating waves from summer to winter. It is expected that the source of the upward propagating waves are in the troposphere (i.e. storms, orographic waves), but it is not as clear what the sources are for the downward propagating waves. The increase in downward propagating waves in winter has been reported in other radiosonde studies (Moffat-Griffin et al., 2013;Yoshiki and Sato, 2000;Moffat-Griffin et al., 2011;Guest et al., 2000;Murphy et al., 2014;Zink and Vincent, 2001a). It is possible that the increase in these downward propagating waves is due to the presence of the stratospheric jet close to South Georgia. Downward propagating waves have also been shown to be generated as a result of partial reflection of waves from an area of high static stability higher in the stratosphere and also from non-linear processes related to large amplitude orographic waves (Sato et al., 2012). To try and determine the likely cause of the downward waves observed in this campaign we examined ERA-Interim zonal winds and looked at the position of the stratospheric jet with respect to South Georgia over two different time periods. From the 13th-17th June the wave profiles are dominated by downward propagating waves, for the 20th -22nd June they are mostly dominated by upward propagating waves. Figure 15 shows the zonal wind at 10 hPa for the following scenarios: (a) The whole time period, (b) the subtraction of the two time periods, (c) 13th-17th June and (d) 20th -22nd June. It can be seen that during the period of downward propagation (Fig, 15c), the jet is strengthened in the 45W-45E sector, with SG lying to the south of the strongest winds in the jet core. During the upward propagation period (Fig. 15d), the strongest winds in the jet have moved eastwards and now lie between 0 and 45E, with weaker winds over South Georgia. Although the data set is limited it does imply that there is a relationship between the position of the stratospheric jet and the dominace of downward propagating waves in the data. It is highly likely that the downward propagating waves in this data are due to the presence of the stratospheric jet over South Georgia.

In the winter there is a known increase in wave activity and it is likely that this increase is due to the strong orographic waves generated by South Georgia. It is also possible that we can see orographic waves generated by the Andes region too, which can travel as far as South Georgia (Alexander and Teitelbaum, 2011;Alexander et al., 2010b;Alexander et al., 2009b).

4.4 Comparisons with the Unified Model

To determine the proportion of energy density and momentum flux due to orographic waves above South Georgia simulations from a high horizontal resolution version of the Unified Model (UM) have been used. Simulations were run with a 1.5 km horizontal resolution (with the lateral boundaries being filled by data from the global UM at 25 km horizontal resolution), the model orography was created from the Shuttle Radar 167 Topography Mission (SRTM) digital terrain dataset (~90 m resolution). There are 118 vertical levels, with the vertical spacing ranging from 500m to 1 km over the lower stratosphere. The model lid was at 78 km but there was a dampling layer applied to the top 20 km. This UM version is designed to capture gravity waves generated due to orography and no gravity wave parameterisations are included (Jackson et al., 2017).

For each radiosonde launch an equivalent profile was created by "flying" a radiosonde through the model data and producing an equivalent profile. Additionally, as the UM and radiosonde data have different height resolutions, a "low resolution" radiosonde profile was created where the radiosonde profile data was interpolated onto the model vertical resolution. The UM and low resolution profiles were then analysed in the same way as the original radiosonde profiles. We focus on the winter campaign as this is when the largest energies and pseudo-momentum fluxes occur and also when strong orographic waves are expected to occur. Figures 16 and 17 show results for the radiosonde, low resolution and UM profiles for kinetic energy density and the zonal pseudo-momentum flux respectively.

In Fig. 16 there is mostly good agreement in the variation of the energy density except where downward waves dominate the radiosonde profiles (at the start and end of the campaign), in these periods the difference between the UM and two radiosonde datasets is larger. This strongly indicates that the large increases we see in the energy density are due to orographic wave activity from South Georgia. The low resolution radiosonde data and UM data are close in agreement during the period where upward waves dominate, the differences can be put down to non-orographic waves also being present in the radiosonde data and in the UM results differences can occur due to small model errors in the wave field accumulating with height (Jackson et al., 2017).

In Fig. 17 there is reasonable agreement in magnitude and direction between the three datasets. Where there is a large deviation in pseudo-momentum flux we see a reduced value from the UM data compared to the two radiosonde values, this is likely due to the same reasons outlined above for Fig. 16. It is interesting to note that during the periods of increased downward wave activity we don't see a major difference between the two datasets, unlike in Fig. 16. This implies that the pseudo-momentum flux is dominated by the upward propagating waves including the orographic waves.

5 Summary

The observed increase in magnitudes of energy density (and thus wave occurrences) and momentum flux from summer to winter is consistent both with satellite observations of the region (Alexander et al., 2009a;Alexander and Grimsdell, 2013;Alexander et al., 2009b;Hindley et al., 2015) and also radiosonde studies of Antarctic and southern mid-latitude locations (Moffat-Griffin et al., 2011;Yoshiki et al., 2004;Yoshiki and Sato, 2000;Moffat-Griffin et al., 2013). An increase of nearly 60% in the magnitude of gravity wave energy density observed from summer to winter is quite striking. Radiosonde data from

the Falkland Islands (which are at a comparable latitude to South Georgia, but has flatter terrain and not as exposed to the strong circumpolar winds) shows an increase in energy density of around 25% from summer to winter (Moffat-Griffin et al., 2013). Macquarie Island sees an increase of around 40% in the summer to winter energy densities. These comparisons show that the results we see are due to a greater generation of gravity waves on South Georgia than on the Falkland Islands or Macquarie Island. The position of South Georgia means that it is exposed to the strong circumpolar winds and storm systems that can generate orographic waves. In the winter the island is exposed to stronger winds, more frequent storms and there are favourable conditions for these orographic waves to reach the stratosphere. Comparisons with the high horizontal resolution UM have provided evidence that the large increases in energy density and momentum fluxes observed in this paper are mainly due to orographic waves from South Georgia.

The increased numbers of downwardly propagating waves observed during the winter (66% of the observed waves compared to 8% in the summer) suggest that there is a stratospheric source in this region. Analysis of ERA-Interim data have shown that the periods when downward waves dominate are coincident with the proximity of the stratospheric jet to South Georgia, making this a likely source of these waves. The horizontal direction of propagation of the waves are generally westward in both campaigns. In the summer though there are more eastward propagating waves. This is likely to be due to filtering effects occurring at lower altitudes. In the winter the wind direction is more constantly eastward, so the majority of waves that reach the stratosphere are westward propagating. In the summer there is more variability in the wind direction so both eastward and westward propagating waves can reach the stratosphere at times.

This study has shown that South Georgia is a strong source of gravity waves. During wintertime the conditions are often favourable for strong orographically generated gravity waves to propagate up to the lower stratosphere. We have shown that the short vertical wavelength waves (observable by the radiosondes) contribute large quantities of energy and momentum to the stratosphere, especially during the winter months. South Georgia is a hotspot of gravity wave activity and it is very likely that it is a main contributor to the "missing" gravity wave momentum flux around the 60°S belt. These results have shown that the momentum flux contributions from South Georgia needs to be included in atmospheric models if they wish to start to rectify the issue of the "missing momentum flux" around 60°S and to improve representations of the duration of the winter Polar Vortex stratospheric temperatures and ozone loss rates.

Acknowledgements

The work was supported by the UK Natural Environment Research Council under grant NE/K012614/1, NE/K012584/1 and NE/K015117/1 (the South Georgia Wave Experiment – SG-WEX).

We would like to thank the government of South Georgia and the South Sandwich Islands and for their co-operation in the delivery of this grant. In addition we would also like to thank the relevant staff at KEP, BAS and University of Bath for all their help in ensuring the successful delivery of the instrument campaigns.

A. C. Moss (who participated in the first radiosonde campaign) was funded by a NERC PhD studentship, and fieldwork was further supported by contributions from the University of Bath and the Royal Meteorological Society Legacy Fund.

References

BAS Meteorological application: http://basmet.nerc-bas.ac.uk/sos/, 2015.

Alexander, M. J., Eckermann, S. D., Broutman, D., and Ma, J.: Momentum flux estimates for South Georgia Island mountain waves in the stratosphere observed via satellite, Geophys. Res. Letts, 36, 10.1029/2009gl038587, 2009a.

Alexander, M. J., Geller, M., McLandress, C., Polavarapu, S., Preusse, P., Sassi, F., Sato, K., Eckermann, S., Ern, M., Hertzog, A., Kawatani, Y., Pulido, M., Shaw, T. A., Sigmond, M., Vincent, R., and Watanabe, S.: Recent developments in gravity-wave effects in climate models and the global distribution of gravity-wave momentum flux from observations and models, Quart. J. R. Met. Soc., 136, 1103-1124, 10.1002/qj.637, 2010a.

Alexander, M. J., and Teitelbaum, H.: Three-dimensional properties of Andes mountain waves observed by satellite: A case study, J. Geophys. Res., 116, D23110, 10.1029/2011jd016151, 2011.

Alexander, M. J., and Grimsdell, A. W.: Seasonal cycle of orographic gravity wave occurrence above small islands in the Southern Hemisphere: Implications for effects on the general circulation, J. Geophys. Res., 118, 10.1002/2013jd020526, 2013.

Alexander, P., Luna, D., Llamedo, P., and de la Torre, A.: A gravity waves study close to the Andes mountains in Patagonia and Antarctica with GPS radio occultation observations, Ann. Geophys., 28, 587-595, 2010b.

Alexander, S. P., Klekociuk, A. R., and Tsuda, T.: Gravity wave and orographic wave activity observed around the Antarctic and Arctic stratospheric vortices by the COSMIC GPS-RO satellite constellation, J. Geophys. Res., 114, D17103, 10.1029/2009jd011851, 2009b.

Allen, S. J., and Vincent, R. A.: Gravity wave activity in the lower atmosphere: Seasonal and latitudinal variations, J. Geophys. Res., 100, 1327-1350, 1995.

Bannister, D.: Fohn winds on South Georgia and their imapct on regional climate, PhD, University of East Anglia, 2015.

Fritts, D. C., and Alexander, M. J.: Gravity wave dynamics and effects in the middle atmosphere, Rev. Geophys., 41, Artn 1003

Doi 10.1029/2001rg000106, 2003.

Fritts, D. C., Vadas, S. L., Wan, K., and Werne, J. A.: Mean and variable forcing of the middle atmosphere by gravity waves, J. Atmos. Sol. Terr. Phys., 68, 247-265, http://dx.doi.org/10.1016/j.jastp.2005.04.010, 2006.

Geller, M. A., and Gong, J.: Gravity wave kinetic, potential, and vertical fluctuation energies as indicators of different frequency gravity waves, J. Geophys. Res., 115, 10.1029/2009jd012266, 2010.

Gong, J., and Geller, M. A.: Vertical fluctuation energy in United States high vertical resolution radiosonde data as an indicator of convective gravity wave sources, Journal of Geophysical Research-Atmospheres, 115, 10.1029/2009jd012265, 2010.

South Georgia and South Sandwich Islands Government webpage: http://www.gov.gs/information/about-sgssi/, 2016.

Guest, F. M., Reeder, M. J., Marks, C. J., and Karoly, D. J.: Inertia–Gravity Waves Observed in the Lower Stratosphere over Macquarie Island, J. Atmos. Sci., 57, 737-752, 10.1175/1520-0469(2000)057<0737:igwoit>2.0.co;2, 2000.

Hindley, N. P., Wright, C. J., Smith, N. D., and Mitchell, N. J.: The southern stratospheric gravity wave hot spot: individual waves and their momentum fluxes measured by COSMIC GPS-RO, Atmos. Chem. Phys., 15, 7797-7818, 10.5194/acp-15-7797-2015, 2015.

Hoffmann, L., Grimsdell, A. W., and Alexander, M. J.: Stratospheric gravity waves at southern hemisphere orographic hotspots: 2003–2014 AIRS/Aqua observations, Atmos. Chem. Phys. Discuss., 2016, 1-30, 10.5194/acp-2016-341, 2016.

Hoskins, B. J., and Hodges, K. I.: A New Perspective on Southern Hemisphere Storm Tracks, J. Clim., 18, 4108-4129, 10.1175/jcli3570.1, 2005.

Innis, J. L., Klekociuk, A. R., and Vincent, R. A.: Interstation correlation of high-latitude lower-stratosphere gravity wave activity: Evidence for planetary wave modulation of gravity waves over Antarctica, Journal of Geophysical Research: Atmospheres, 109, n/a-n/a, 10.1029/2004JD004961, 2004.

Jackson, D. R., Gadian, A., Hoffmann, L., Hughes, J., King, J., Moffat-Griffin, T., Moss, A. C., Ross, A. N., Vosper, S. B., Wright, C. J., and Mitchell, N.: SG-WEX – a platform for improved analysis of gravity waves and low-level wind impacts generated from mountainous islands, Bull. Amer. Met. Soc, 2017.

Jewtoukoff, V., Hertzog, A., Plougonven, R., de la Camara, A., and Lott, F.: Comparison of Gravity Waves in the Southern Hemisphere Derived from Balloon Observations and the ECMWF Analyses, J. Atmos. Sci., 72, 3449-3468, 10.1175/jas-d-14-0324.1, 2015.

McLandress, C., Shepherd, T. G., Polavarapu, S., and Beagley, S. R.: Is Missing Orographic Gravity Wave Drag near 60 degrees S the Cause of the Stratospheric Zonal Wind Biases in Chemistry Climate Models?, J. Atmos. Sci., 69, 802-818, 10.1175/jas-d-11-0159.1, 2012.

Moffat-Griffin, T., Hibbins, R. E., Jarvis, M. J., and Colwell, S. R.: Seasonal variations of gravity wave activity in the lower stratosphere over an Antarctic Peninsula station, J. Geophys. Res., 116, D14111, doi:10.1029/2010JD015349, 2011.

Moffat-Griffin, T., Jarvis, M. J., Colwell, S. R., Kavanagh, A. J., Manney, G. L., and Daffer, W. H.: Seasonal variations in lower stratospheric gravity wave energy above the Falkland Islands, J. Geophys. Res., 118, 10861-10869, 10.1002/jgrd.50859, 2013.

Murphy, D. J., Alexander, S. P., Klekociuk, A. R., Love, P. T., and Vincent, R. A.: Radiosonde observations of gravity waves in the lower stratosphere over Davis, Antarctica, J. Geophys. Res., 119, 11,973-911,996, 10.1002/2014JD022448, 2014.

Nastrom, G. D., Van Zandt, T. E., and Warnock, J. M.: Vertical wavenumber spectra of wind and temperature from high-resolution balloon soundings over Illinois, J. Geophys. Res., 102, 6685-6701, 10.1029/96JD03784, 1997.

Sato, K., and Yoshiki, M.: Gravity Wave Generation around the Polar Vortex in the Stratosphere Revealed by 3-Hourly Radiosonde Observations at Syowa Station, J. Atmos. Sci., 65, 3719-3735, 10.1175/2008jas2539.1, 2008.

Sato, K., Tateno, S., Watanabe, S., and Kawatani, Y.: Gravity Wave Characteristics in the Southern Hemisphere Revealed by a High-Resolution Middle-Atmosphere General Circulation Model, J. Atmos. Sci., 69, 1378-1396, 10.1175/jas-d-11-0101.1, 2012.

Smith, R. B., Woods, B. K., Jensen, J., Cooper, W. A., Doyle, J. D., Jiang, Q., and Grubisic, V.: Mountain waves entering the stratosphere, J. Atmos. Sci., 65, 2543-2562, 10.1175/2007jas2598.1, 2008.

Torrence, C., and Compo, G. P.: A practical guide to wavelet analysis, Bull. Amer. Met. Soc, 79, 61-78, 1998.

RS92-SGP Datasheet: http://www.vaisala.com/en/products/soundingsystemsandradiosondes/radiosondes/Pages/RS92.aspx, 2013.

Vincent, R., Allen, S. J., and Eckermann, E.: Gravity-wave parameters in the lower stratosphere, in: Gravity Wave Processes: Their Parameterization in Global Climate Models, edited by: Hamilton, K., Springer-Verlag, New York, 7-25, 1997.

Wang, L., and Geller, M. A.: Morphology of gravity-wave energy as observed from 4 years (1998–2001) of high vertical resolution U.S. radiosonde data, J. Geophys. Res., 108, n/a-n/a, 10.1029/2002JD002786, 2003.

Whiteway, J. A., and Duck, T. J.: Evidence for critical level filtering of atmospheric gravity waves, Geophys. Res. Lett., 23, 145-148, 10.1029/95GL03784, 1996.

Wright, C. J., Hindley, N. P., Moss, A. C., and Mitchell, N. J.: Multi-instrument gravity-wave measurements over Tierra del Fuego and the Drake Passage – Part 1: Potential energies and vertical wavelengths from AIRS, COSMIC, HIRDLS, MLS-Aura, SAAMER, SABER and radiosondes, Atmos. Meas. Tech., 9, 877-908, 10.5194/amt-9-877-2016, 2016.

Yoshiki, M., and Sato, K.: A statistical study of gravity waves in the polar regions based on operational radiosonde data, J. Geophys. Res., 105, 17,995-918,011, 2000.

Yoshiki, M., Kizu, N., and Sato, K.: Energy enhancements of gravity waves in the Antarctic lower stratosphere associated with variations in the polar vortex and tropospheric disturbances, J. Geophys. Res., 109, doi:10.1029/2004JD004870, 2004.

Zhang, S. D., Yi, F., Huang, C. M., and Huang, K. M.: High vertical resolution analyses of gravity waves and turbulence at a midlatitude station, J. Geophys. Res., 117, 2156-2202, 10.1029/2011JD016587, 2012.

Zink, F., and Vincent, R. A.: Wavelet analysis of stratospheric gravity wave packets over Macquarie Island 1. Wave parameters, J. Geophys. Res., 106, 10,275-210,288, 2001a.

Figure 1. Map of location of South Georgia

Figure 2. Topographic map of South Georgia, showing the largest mountains and locations around the island (Bannister, 2015)

Figure 3. Temperature profiles for the summer (a) and winter (b) radiosonde campaigns. Each temperature profile is separated by 20K.

Figure 4. Radiosonde balloon trajectories for the summer (left) and winter (right) campaigns. Green diamond marks the location of KEP.

Figure 5. Example of temperature and wind profile fitting for 13th June 11 am launch. The top row of figures show the temperature profile between 12 km and 25 km with a 3rd order polynomial fit and the residual temperature. The bottom row shows the same but for the wind speed profile.

Figure 6. Example hodograph using data from 17th June 9 am launch

Figure 7. The kinetic, potential and vertical energy densities during the summer campaign.

Figure 8. As Figure 7 but for the winter campaign.

Figure 9. Era40 summer wind plots above KEP (a) shows zonal wind (positive eastwards), (b) meridional wind (positive northwards).

Figure 10. As Figure 9 but for winter.

Figure 11. Zonal (top) and meridional (bottom) pseudo-momentum flux from the summer campaign.

Figure 12. As Figure 11 but for the winter campaign.

Figure 13. The horizontal direction of propagation of individual gravity waves in the summer campaign data. The left plot is for downward propagating waves, the right plot is for upward propagating waves.

Figure 14. As Figure 13 but for the winter campaign data.

Figure 15. ERA Interim zonal wind at 10 hPa: (a) 13th-22nd June, (b) c and d subtracted (c) 13th-17th June and (d) 20th-22nd June.

Figure 16. Kinetic energy density calculated using winter campaign radiosonde data (black solid line), Unified model data (blue dashed line) and low resolution radiosonde data (red dot dash line).

Figure 17. Zonal pseudo-momentum flux calculated using winter campaign radiosonde data (black solid line), Unified model data (blue dashed line) and low resolution radiosonde data (red dot dash line).

Table 1: Pseudo-momentum flux summer and winter measurements from South Georgia and Macquarie Island.

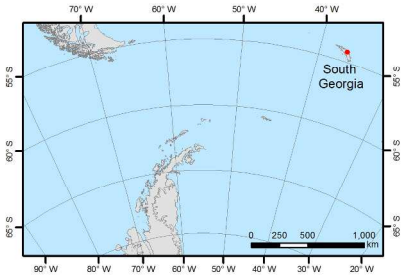

Figure 1: Map of location of South Georgia.

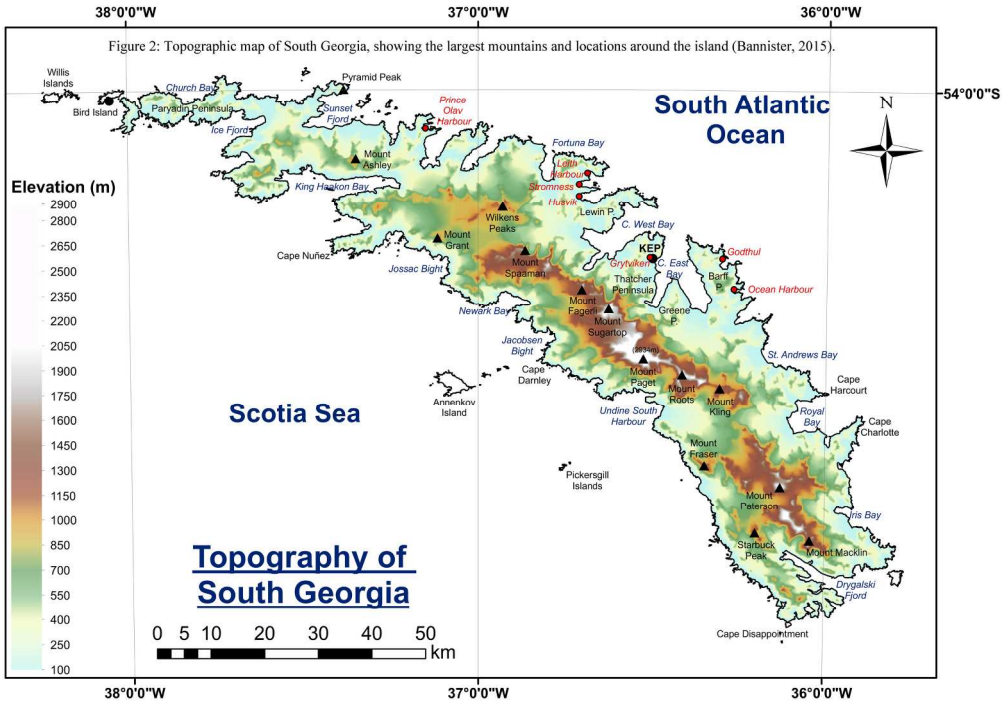

Figure 2: Topographic map of South Georgia, showing the largest mountains and locations around the island (Bannister, 2015).

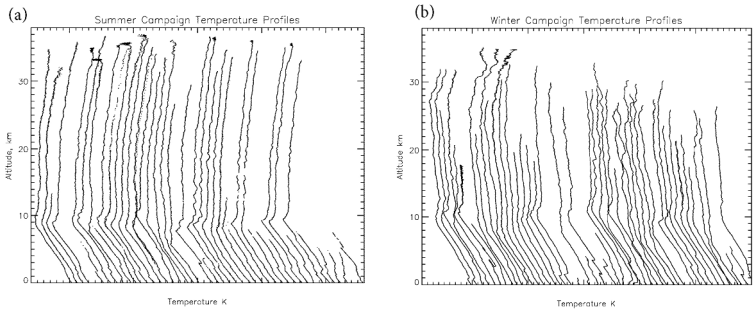

Figure 3: Temperature profiles for the summer (a) and winter (b) radiosonde campaigns. Each temperature profile is separated by 20 K.

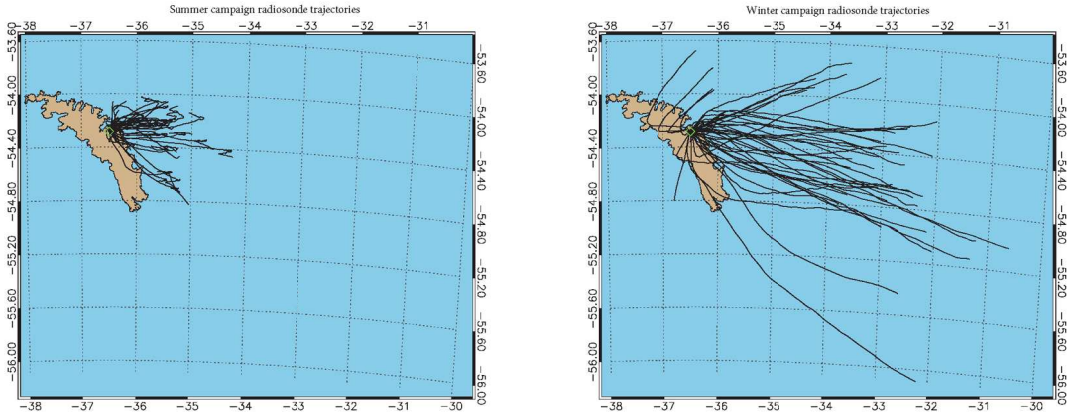

Figure 4: Radiosonde balloon trajectories for the summer (left) and winter (right) campaigns. Green diamond marks the location of KEP.

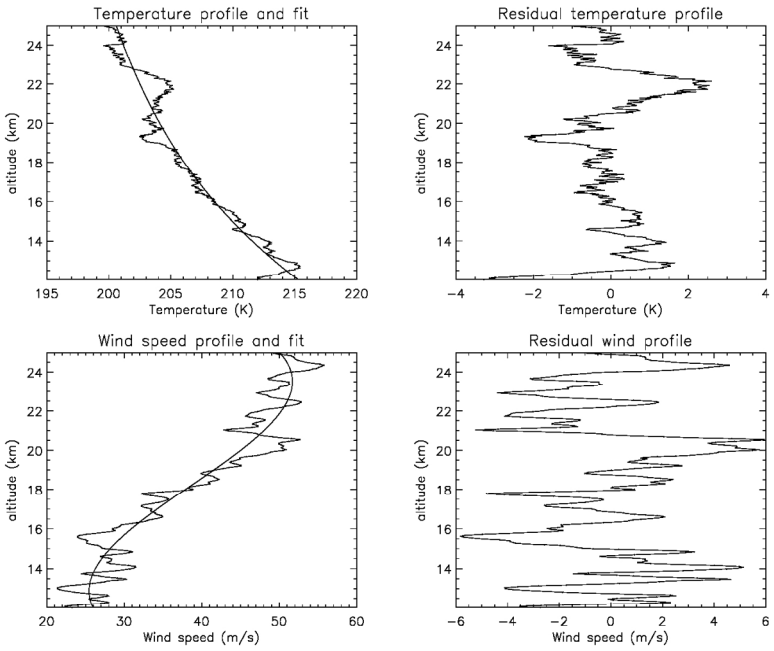

Figure 5: Example of temperature and wind profile fitting for 13th June 11am launch. The top row of figures show the temperature profile between 12 km and 25 km with a 3rd-order polynomial fit and the residual temperature. The bottom row shows the same but for the wind speed profile.

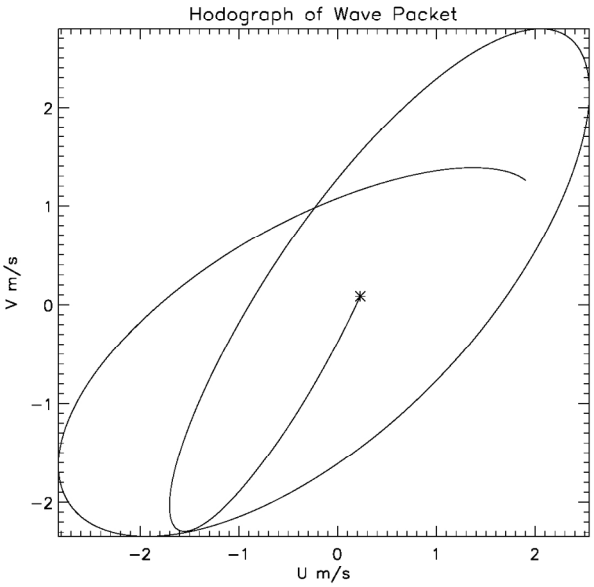

Figure 6: Example hodograph using data from 17th June 9am launch.

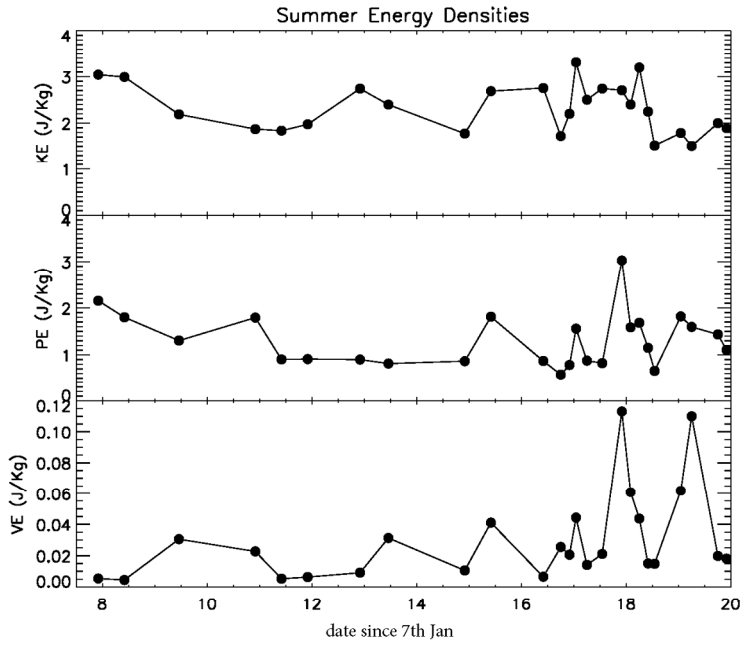

Figure 7: The kinetic, potential and vertical energy densities during the summer campaign.

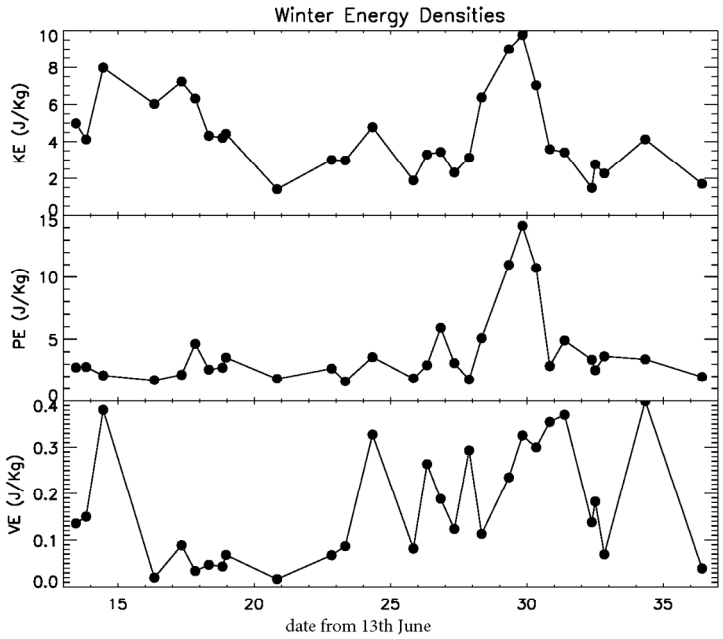

Figure 8: As Figure 7 but for the winter campaign.

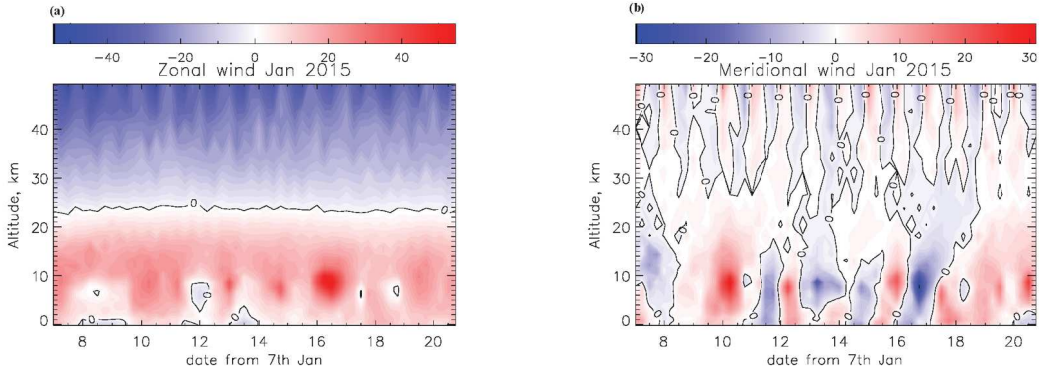

Figure 9: Era40 summer wind plots above KEP; (a) shows zonal wind (positive eastwards), (b) meridional wind (positive northwards).

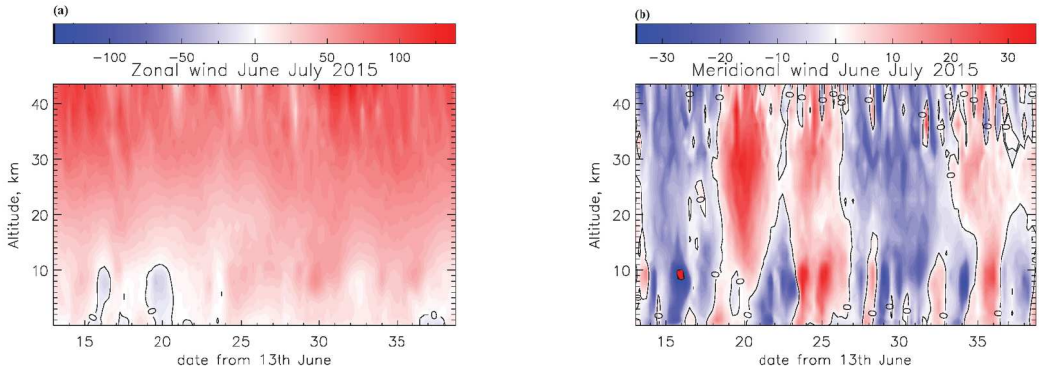

Figure 10: As Figure 9 but for winter.

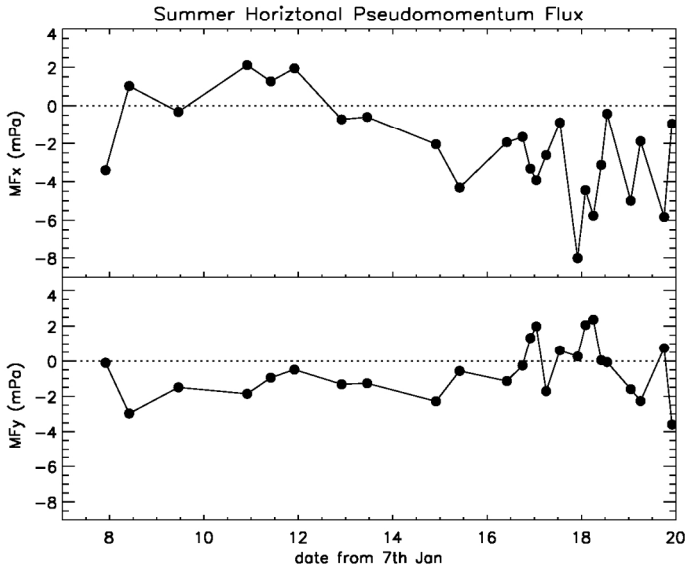

Figure 11: Zonal (top) and meridional (bottom) pseudo-momentum flux from the sumeer campaign.

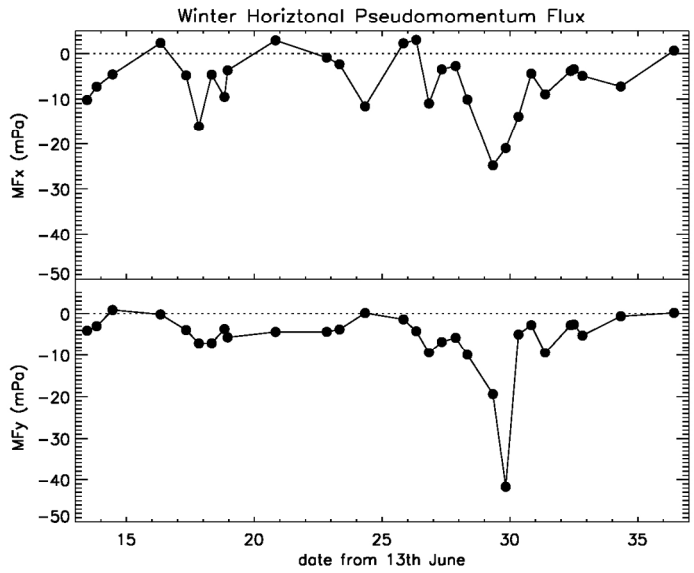

Figure 12: As for Figure 11 but for the winter campaign

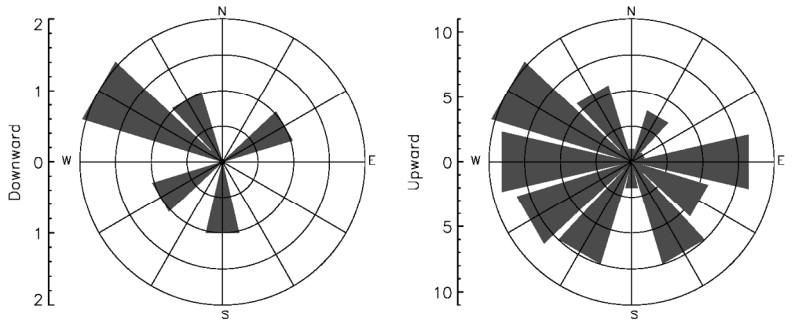

Figure 13: The horizontal direction of propagation of individual gravity waves in the summer campaign data. The left plot is for downward propagating waves, the right plot is for upward propagating waves.

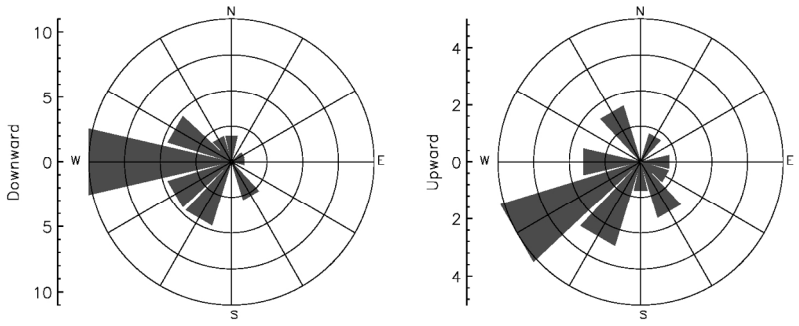

Figure 14: As for Figure 13 but for the winter campaign data.

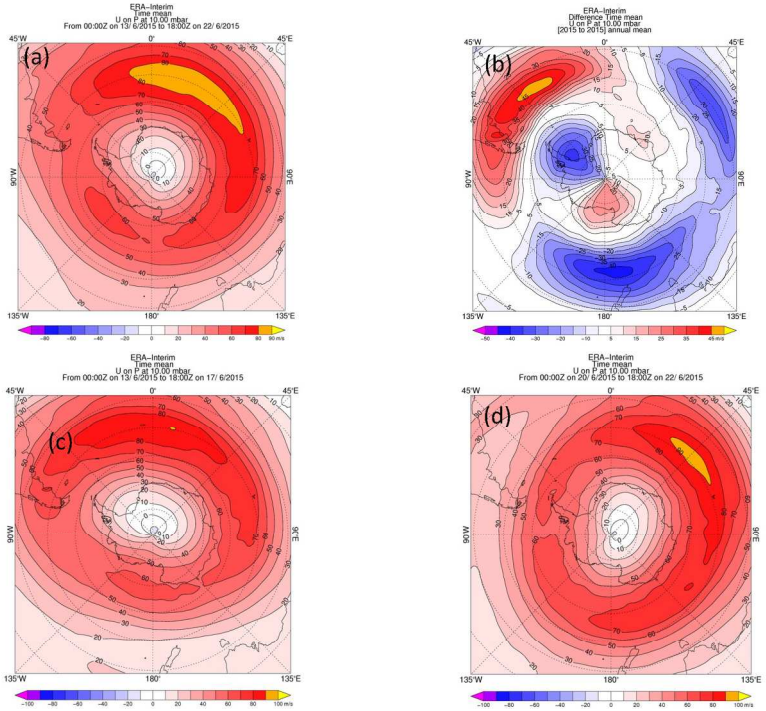

Figure 15: ERA Interim zonal wind at 10 hPa: (a) 13th-22nd June, (b) c and d subtracted (c) 13th-17th June and (d) 20th -22nd June.

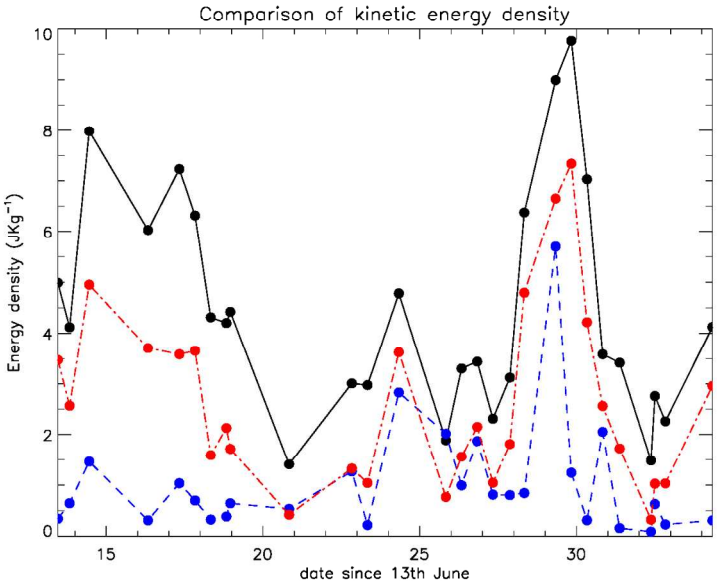

Figure 16: kinetic energy density calculated using winter campaign radiosonde data (black solid line), Unified model data (blue dashed line) and low resolution radiosonde data (red dot-dash line).

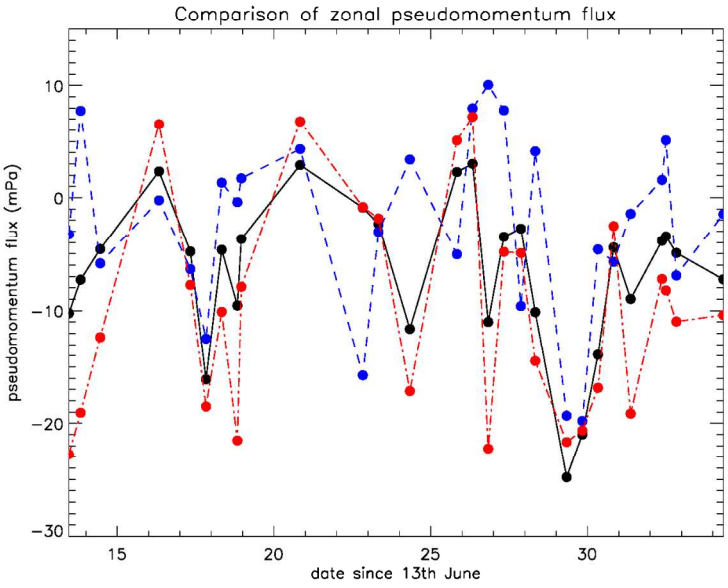

Figure 17: zonal pseudo-momentum flux calculated using winter campaign radiosonde data (black solid line), Unified model data (blue dashed line) and low resolution radiosonde data (red dot-dash line).